Acta Crystallographica Section D
Biological Crystallography
ISSN 0907-4449

Flexibility of the Cu,Zn superoxide dismutase structure investigated at 0.57 GPa

Isabella Ascone,[a,b]* Carmelinda Savino,[c] Richard Kahn[d] and Roger Fourme[b]

[a]ENSCP, UMR CNRS 7223, 11 Rue Pierre et Marie Curie, 75231 Paris CEDEX 05, France, [b]Synchrotron SOLEIL, BP48 Saint Aubin, 91192 Gif-sur-Yvette, France, [c]Istituto di Biologia e Patologia Molecolari, CNR, c/o Dipartimento di Scienze Biochimiche, University of Rome La Sapienza, Piazzale Aldo Moro 5, 00185 Rome, Italy, and [d]IBS, 41 Rue Jules Horowitz, 38027 Grenoble, France

Correspondence e-mail: isabella-ascone@chimie-paristech.fr

Received 27 January 2010
Accepted 1 April 2010

PDB Reference: CuZnSOD at 0.57 GPa, 3hw7.

The 2 Å resolution crystal structure of bovine erythrocyte Cu,Zn superoxide dismutase (CuZnSOD) has been determined by X-ray diffraction at high pressure (0.57 GPa) and room temperature. At 0.57 GPa the secondary, tertiary and quaternary structures are similar to other previously determined bovine erythrocyte CuZnSOD structures. Nevertheless, pressure has a localized impact on the atomic coordinates of C^{α} atoms and on side chains. The compression of the crystal and of the protein backbone is anisotropic. This anisotropy is discussed, taking into account intermolecular contacts and protein conformation. Pressure perturbation highlights the more flexible zones in the protein such as the electrostatic loop. At 0.57 GPa, a global shift of the dimetallic sites in both subunits and changes in the oxidation state of Cu were observed. The flexibility of the electrostatic loop may be useful for the interaction of different metal carriers in the copper-uptake process, whereas the flexibility of the metal sites involved in the activity of the protein could contribute to explaining the ubiquitous character of CuZnSODs, which are found in organisms living in very different conditions, including the deep-sea environment. This work illustrates the potential of combining X-ray crystallography with high pressure to promote and stabilize higher energy conformational substates.

1. Introduction

Superoxide dismutases, which catalyse the dismutation of two superoxide radicals into dioxygen and hydrogen peroxide, are metalloproteins that are found in all oxygen-utilizing organisms so far examined and have been implicated in protection against a variety of types of damage (Fridovich, 1975). They may bind either copper and zinc, manganese or iron at the active-site centre; the functional enzyme is a 32 kDa homodimer. This article is dedicated to bovine erythrocyte Cu,Zn superoxide dismutase (CuZnSOD). The crystal structure of this protein at 2 Å resolution (Tainer *et al.*, 1982) provided a detailed description of the enzyme. The tertiary structure is based on an antiparallel Greek-key β-barrel topology composed of two β-sheets of four β-strands each connected by three long external loops.

The contact area across the twofold axis is broad and closely fitted. It involves part of the outside surface of the β-barrel, the last few residues at the C-terminus and the disulfide loop.

Table 1
Refinement parameters and results of the final refinement.

Values in parentheses are for the highest resolution shell.

PDB code	3hw7
Data collection	
Space group	$P2_12_12_1$
Unit-cell parameters (Å, °)	a = 46.85, b = 50.51, c = 146.38
Resolution (Å)	2.00 (2.11–2.00)
Completeness (%)	91.0 (83.1)
Multiplicity	5.8 (4.7)
$R_{\rm merge}$† (%)	11.1 (31.3)
$I/\sigma(I)$	11.5 (4.6)
No. of reflections	22012 (2893)
Refinement	
Resolution (Å)	19.89–2.00
No. of atoms	
Protein, chain A/B	1094/1094
Cu, chain A/B	1/1
Zn, chain A/B	1/1
Water molecules	206
$R_{\rm cryst}/R_{\rm free}$‡ (%)	17.2/21.8
Estimated standard uncertainty based on maximum likelihood (Å)	0.097
DPI	0.15
R.m.s. deviations	
Bonds (Å)	0.014
Angles (°)	1.513
Ramachandran plot (%)	
Core	90.7
Allowed	9.3
Generous	0.0
Disallowed	0.0

† $R_{\rm merge} = \sum_{hkl}\sum_i |I_i(hkl) - \langle I(hkl)\rangle| / \sum_{hkl}\sum_i I_i(hkl)$. ‡ $R_{\rm cryst} = \sum_{hkl} \big||F_{\rm obs}| - |F_{\rm calc}|\big| / \sum_{hkl} |F_{\rm obs}|$, where $|F_{\rm obs}| > 0$. $R_{\rm free}$ is based on 5.1% of the data that were randomly selected and were not used in the refinement.

It principally consists of hydrophobic side-chain interactions: there are four hydrogen bonds between subunits, while 14 hydrophobic side groups from each subunit are involved in van der Waals contacts (Tainer *et al.*, 1982).

CuZnSOD is one of the most thermally stable enzymes known in mesophilic organisms. Dismutase activity declines at 353 K, with a corresponding melting temperature of above 363 K. The protein is stable in strong denaturants: activity is observed in 4% SDS or 10 *M* urea. Furthermore, as discussed later in this article, the enzyme is very stable under high pressure. However, it has been shown that non-native conformational changes arising from mutations in the metal-binding region permit an increase in the interaction between dimers that facilitates protein polymerization, which has been associated with neurodegenerative disorders (Nordlund & Oliveberg, 2006).

Recent instrumental and methodological developments in high-pressure macromolecular crystallography have allowed the collection of complete and accurate diffraction data from compressed samples, even in the case of crystals belonging to low-symmetry space groups (Fourme *et al.*, 2001, 2006, 2009; Girard *et al.*, 2007).

Here, we present a single-crystal X-ray diffraction study of CuZnSOD in space group $P2_12_12_1$ at 0.57 GPa and room temperature. The crystal structure (hpSOD) was determined and refined at 2 Å resolution. The structural basis of the remarkable stability of this dimeric protein and the flexibility of particular regions highlighted by pressure perturbation are among the main questions addressed in this article.

2. Experimental

The instrumentation and experimental procedures for high-pressure macromolecular crystallography (HPMX) experiments on ESRF beamlines ID30 and ID27 have been described elsewhere (Fourme *et al.*, 2001; Girard *et al.*, 2007). CuZnSOD was prepared as described previously (Ascone *et al.*, 2005). CuZnSOD crystals (space group $P2_12_12_1$) were grown at 291 K in protein solution (15 mg ml^{-1}) containing 7.5% PEG 4000, 50 m*M* NaCl, 50 m*M* sodium cacodylate buffer and 7.5% 1,4-dioxane. Copper gaskets were used. Data were collected at 295 K and 0.57 GPa with 1° oscillations and a typical exposure time of 45 s per frame. As the experiments were performed at room temperature, each crystal was translated by about 50 µm after an oscillation of a few degrees in order to successively irradiate different parts of the sample. Data were integrated using *XDS* (Kabsch, 1993). The integrated intensities were scaled and merged using *SCALA* from the *CCP*4 suite of programs (Collaborative Computational Project, Number 4, 1994). The data-processing statistics are summarized in Table 1. 21 970 reflections in the resolution range 2.0–19.9 Å were used in refinement and the completeness was 91.0%. The starting molecular model for refinement of the high-pressure structure was built from PDB entry 1cbj (CuZnSOD at 1.65 Å resolution in space group $P2_12_12_1$ at room temperature and atmospheric pressure; rtSOD; Hough & Hasnain, 1999).

Refinement was performed using *REFMAC*5 (Murshudov *et al.*, 1997) from the *CCP*4 package. The final $R_{\rm cryst}$ and $R_{\rm free}$ values were 17.2% and 21.8%, respectively. All solvent molecules and ions were removed in an initial cycle. The $R_{\rm free}$ value was based on randomly selected reflections corresponding to 5.1% of the complete data. The r.m.s. deviations from ideal values for bond lengths and bond angles were 0.014 Å and 1.513°, respectively. Secondary-structure assignment was performed using a standard method (Kabsch & Sander, 1983) and the geometrical quality of the model was assessed using *PROCHECK* (Laskowski *et al.*, 1993).

The structure was refined without noncrystallographic symmetry (NCS) restraints. The graphics program *Coot* (Emsley & Cowtan, 2004) was used to visualize ($2F_{\rm obs} - F_{\rm calc}$) and ($F_{\rm obs} - F_{\rm calc}$) difference maps. Comparative analysis between hpSOD and models was performed by superposing secondary-structure elements (*SSM* procedure; Schneider, 2002).

Pockets were investigated using *CASTp* (Dundas *et al.*, 2006) with a probe of radius 1.4 Å, which is the standard dimension used to approximate the size of a water molecule. The volumes and surface areas of hpSOD, rtSOD and ltSOD (fully reduced CuZnSOD at 100 K) were calculated using *Swiss-PdbViewer* (Guex & Peitsch, 1997) considering main and side chains plus Cu and Zn ions without water molecules.

The coordinates of hpSOD have been deposited in the Protein Data Bank (accession code 3hw7).

3. Results

3.1. Unit-cell compression at 0.57 GPa and its anisotropy

Early HPMX studies (Fourme *et al.*, 2001) allowed the measurement of the unit-cell parameters of CuZnSOD up to 1 GPa. In this pressure range the space group is unchanged and there is no noticeable variation in the diffraction power.

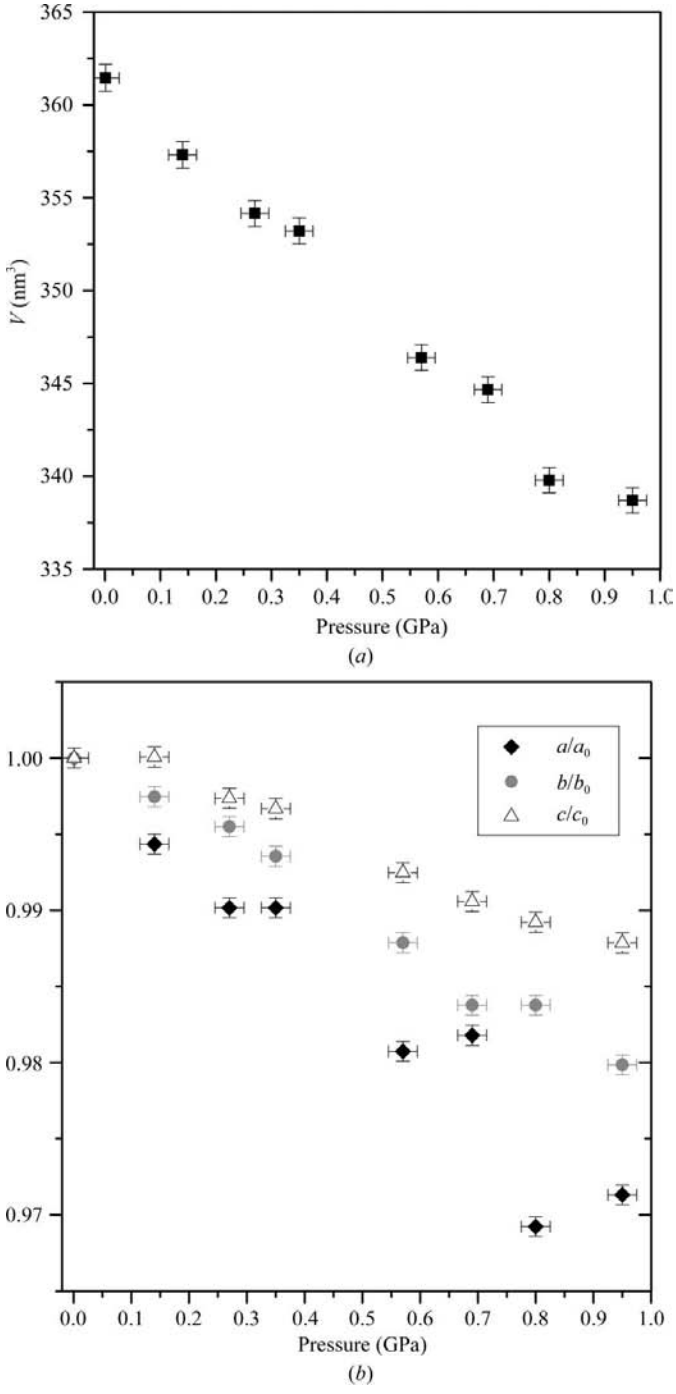

Figure 1
Data obtained from the compressibility experiment (squares) and from hpSOD (circles). (*a*) Unit-cell volume and (*b*) relative length of the unit-cell parameters of the orthorhombic CuZnSOD crystal as a function of pressure.

Crystal stability extends beyond 1 GPa as diffraction was once observed up to about 1.2 GPa; at this point the crystal was destroyed by an accidental pressure jump. The stability of CuZnSOD crystals to at least 1 GPa implies that the dimeric molecule retains its tertiary and quaternary structure in this pressure range.

Fig. 1(*a*) shows the variation in the unit-cell volume of the orthorhombic CuZnSOD crystal as a function of pressure. At about 1 GPa the relative variations of the unit-cell parameters *a*, *b* and *c* (Fig. 1*b*) are −2.9%, −2.0% and −1.2%, respectively, showing an anisotropic compression, and the relative variation of the unit-cell volume is −6.7%. The unit-cell parameters at 0.57 GPa are $a = 46.85$, $b = 50.51$, $c = 146.38$ Å.

Figs. 1(*a*) and 1(*b*) show that the unit-cell volume and parameters at 0.57 GPa are in a good agreement with the previous compressibility experiment. The contraction of the *b* and *c* axes is linear; the contraction of the *a* axis is roughly linear, but a meaningful deviation from linearity is observed between 0.7 and 0.8 GPa.

The compression of tetragonal lysozyme (tHEWL) is nearly linear and the relative volume variation extrapolated to 1 GPa is −9.4%. This value is strikingly large compared with the compressibility of the CuZnSOD crystals. A hypothesis on the origin of these differences and an extended discussion about

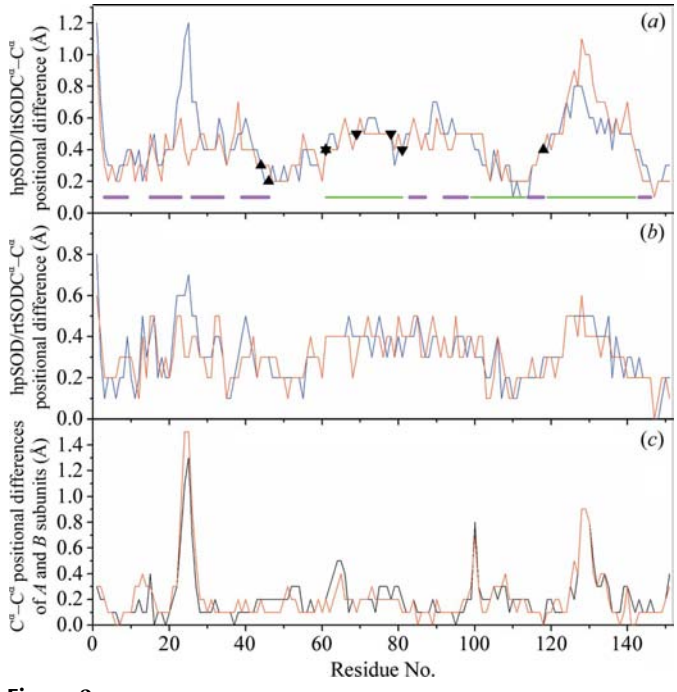

Figure 2
Positional differences between superposed C$^{\alpha}$ atoms of hpSOD and the models. Subunits are indicated in different colours: the *A* subunit is in red and the *B* subunit is in blue. (*a*) Superposition of the secondary-structure elements of hpSOD and ltSOD. Equivalent secondary-structure elements are indicated in magenta (strands) and green (loops). Zn and Cu ligands are indicated by triangles (pointing down and pointing up, respectively). (*b*) Superposition of the secondary-structure elements of hpSOD and rtSOD. (*c*) Positional differences between superposed C$^{\alpha}$ atoms obtained by superposing the secondary-structure elements of the *A* and *B* subunits: the superposition for hpSOD is shown in red and that for rtSOD is shown in black.

the compressibility of several macromolecular crystals and macromolecules can be found in a separate article (Ascone *et al.*, 2010).

3.2. Three-dimensional structure at 0.57 GPa and comparison with published structures

The secondary and tertiary structures of the dimer at 0.57 GPa are similar to previously determined bovine erythrocyte CuZnSOD structures. Each subunit (*A* and *B*) presents the conventional scaffold consisting of an eight-stranded β-barrel and three external loops defined by residues His61–Leu82 (loop 1), Asp99–Arg113 (loop 2) and Glu119–Leu142 (loop 3). Loop 3 (Fig. 2*a*) is also called the electrostatic loop and contains several highly conserved charged residues (Teh *et al.*, 2008).

In order to investigate pressure effects in detail, hpSOD was compared with two orthorhombic $P2_12_12_1$ structures from the PDB: 1cbj (rtSOD; Hough & Hasnain, 1999) and 1q0e (ltSOD; Hough & Hasnain, 2003). The rtSOD structure was determined at room temperature to 1.65 Å resolution, with one Cu site oxidized and the other reduced, while ltSOD is a 1.15 Å resolution structure of the fully reduced protein at 100 K. These structures allow pressure effects to be monitored independently of copper oxidation state and temperature effects. We also used the structure of Co-substituted bovine erythrocyte superoxide dismutase (CuCoSOD) determined at 2.0 Å resolution at 277 K (PDB code 1cob; Djinovic *et al.*, 1992) in order to compare bond and contact distances with the same uncertainty as in hpSOD.

A comparison of rtSOD and ltSOD, which have different copper oxidation states and were determined at very different temperatures at atmospheric pressure, has previously been performed (Hough & Hasnain, 2003). The average positional difference is 0.24 Å, with a large number of differences in the range 0.1–0.2 Å. Larger average values have been identified for momomer *A* around residue 130 (of up to 0.8 Å) and for monomer *B* around residue 25 (of up to 0.9 Å). These differences were in part assumed to reflect structural changes as a result of freezing and the accuracy of the structure determination (Hough & Hasnain, 2003). However, if rtSOD is compared with a structure (PDB code 1e9o; Hough *et al.*, 2000) that has a similar copper environment and was determined under similar experimental conditions (pressure, temperature and resolution) the plot of the average C^{α} positional difference (*SSM* procedure) is lower than 0.1 Å (Supplementary Fig. S1[1]). Superposition (*SSM* procedure) of hpSOD onto the rtSOD and ltSOD models shows that all 302 residues of the two subunits match, with average r.m.s. $C^{\alpha}-C^{\alpha}$ differences of 0.33 and 0.47 Å, respectively. Comparisons are given for the *A* and *B* subunits in hpSOD and ltSOD (Fig. 2*a*) and in hpSOD and rtSOD (Fig. 2*b*). Secondary-structure elements (eight strands and three loops) are indicated in Fig. 2(*a*). In Figs. 2(*a*) and 2(*b*) a similar pattern is obtained in which segments (5–10, 49–55, 109–113 and 144–151) that are nearly invariant (differences of $\leq$0.25 Å) separate three regions in which the r.m.s. positional differences for equivalent C^{α} atoms are larger. The differences in the most variable regions, around residue 25 in subunit *B* and residue 130 in subunit *A*, in Fig. 2(*a*) are greater with respect to those in Fig. 2(*b*), with the largest values being 1.2 and 1.1 Å, respectively. It is noteworthy that some strands are scarcely perturbed by pressure (strands 1, 4, 7 and 8), whereas this is not the case for others (strands 2, 3, 5 and 6). Similarly, the first and third loops are more affected by pressure than the second loop. At high pressure the asymmetric displacement of the electrostatic loop already observed at low temperature in subunit *A* is amplified and extended to the *B* subunit. Consequently, high pressure highlights the structural flexibility of particular regions.

Moreover, the similar patterns in Figs. 2(*a*) and 2(*b*) for both subunits indicate that the structural differences are independent of the oxidation state of the protein. In order to confirm this result, hpSOD was compared with three other crystal structures, 1e9p, 1e9q and 1e9o, at 1.70, 1.75 and 1.85 Å resolution, respectively, which are isomorphous with rtSOD and have several conformations for the reduced Cu site in the *A* subunit (Hough *et al.*, 2000). Plots of positional differences between equivalent C^{α} atoms *versus* residue number after least-squares superposition of hpSOD onto these structures show the pattern previously described for Figs. 2(*a*) and 2(*b*): the displacements of C^{α} atoms with respect to the reference depend on the regions in the residue sequences (see Supplementary Figs. S2, S3 and S4[1]).

Table 2 shows volume and surface values for the dimer and the monomers in hpSOD, CuCoSOD, rtSOD and ltSOD. Structures at atmospheric pressure have somewhat different volume and surface values depending on the resolution and on the conformation of side chains at the protein surface. The volumes of the dimer and of each monomer in hpSOD are smaller compared with the reference structures (dimer volume

Table 2
Volumes and surfaces of the dimer and subunits for hpSOD, CuCoSOD, rtSOD and ltSOD.

Calculations were performed considering the main chain, side chains and the two ions without water molecules.

	hpSOD	CuCoSOD	rtSOD	ltSOD
Dimer volume (Å^3)	35004	35392	35816	36219
Dimer area (Å^2)	11015	11458	11321	11586
Volume, *A* subunit (Å^3)	17310	17521	17745	17816
Area, *A* subunit (Å^2)	5872	6048	5991	6137
Volume, *B* subunit (Å^3)	17314	17414	17644	17953
Area, *B* subunit (Å^2)	5875	6061	6032	6130

Table 3
Subunit-to-subunit backbone hydrogen bonds (Å) as observed in hpSOD and reference structures.

		hpSOD	rtSOD	ltSOD	CuCoSOD
Gly49*A* N	Ile149*B* O	2.79	2.75	2.85	2.76
Gly112*A* O	Ile149*B* N	2.79	2.82	2.87	2.92
Ile149*A* O	Gly49*B* N	2.76	2.77	2.84	2.68
Ile149*A* N	Gly112*B* O	2.79	2.82	2.88	2.86

[1] Supplementary material has been deposited in the IUCr electronic archive (Reference: BE5147). Services for accessing this material are described at the back of the journal.

variation of −1.1%, −2.2% and −3.3% with respect to CuCoSOD, rtSOD and ltSOD, respectively), indicating that the protein is more compact under pressure. This volume variation allows the calculation of the molecular isothermal compressibility of the 'dry' macromolecule. The value calculated using

$$\kappa_T = -\frac{1}{V}\left(\frac{\partial V}{\partial P}\right)_T \quad (1)$$

with rtSOD or ltSOD as a reference was 0.040 or 0.059 GPa^{-1}, respectively. A more accurate determination may be possible using a reference structure at atmospheric pressure determined under the same experimental conditions.

3.3. Effect of pressure on pockets at the protein surface

The bovine CuZnSOD structure is very compact and lacks the large internal cavities that have been identified in many other proteins, for example myoglobin and other globins (Vallone *et al.*, 2004). No internal cavities were identified in rtSOD and ltSOD. At 0.57 GPa, the whole protein structure is compressed and two small internal cavities, one in each subunit, are formed in the proximity of the S—S bond. Two main pockets are localized around the subunit interface. For rtSOD, their volumes are 1106 and 572 $Å^3$ and for ltSOD 947 and 594 $Å^3$. In hpSOD, these values are reduced to 747 and 407 $Å^3$. The fractional volume variations are −32.4% and −28.8%, respectively, compared with rtSOD and −21.5% and −31.5% compared with ltSOD. From visual inspection of these main pockets, the volume decrease arises from an overall displacement of all side chains. The surface of the two subunits presents smaller pockets. Their total volume is 953 $Å^3$ for rtSOD and 876 $Å^3$ for hpSOD (−8.1%). In conclusion, pressure produces a non-uniform contraction of all cavities and the pocket contraction is larger for the two main pockets in the proximity of the subunit interface.

3.4. Interactions between the *A* and *B* subunits in the dimer at 0.57 GPa

The eukaryotic CuZnSODs are found as functional dimers in solution. In the crystalline state, all enzymes of this family described to date display a tight and stable dimeric structure based on a conserved subunit interface contact area. Stability is established by a number of evolutionary invariant or highly conserved residues allowing the formation of a dimeric species with a quasi-twofold axis relating the two polypeptide chains. The subunit interface is formed by 19 residues contributed by three β-strands, by the S—S subloop, by the Greek-key loop and by the C-terminal region. Stability is mostly ensured by hydrophobic side-chain interactions. There are only four main-chain-to-main-chain hydrogen bonds between the two subunits.

At 0.57 GPa, the atomic positions of amino-acid residues at (or near) the dimer interface are almost unaffected by pressure. The relevant segments are 9–11, 49–53, 111–113 and 146–149; they correspond to the minima in the curves in Figs. 2(*a*) and 2(*b*), indicating that the C^α positional differences are $\leq$0.25 Å for these regions.

Most side chains at the subunit interface are nearly superposed (positional difference of 0.1–0.2 Å) on corresponding residues of ltSOD (*e.g.* Ile149*A*, Ile149*B*, Ile111*A*, Ile111*B*, Val146*A*, Val146*B* *etc.*). Amino acids close to the interface region also show small displacements of C^α and lateral chain positions at high pressure compared with the rtSOD and ltSOD models. This is observed in particular for the polar Lys151 and the hydrophobic Phe48 in both subunits. van der Waals contacts are not significantly modified at high pressure.

The four main-chain-to-main-chain hydrogen-bond lengths between the two subunits for hpSOD, rtSOD, ltSOD and CuCoSOD are reported in Table 3. These values are rather

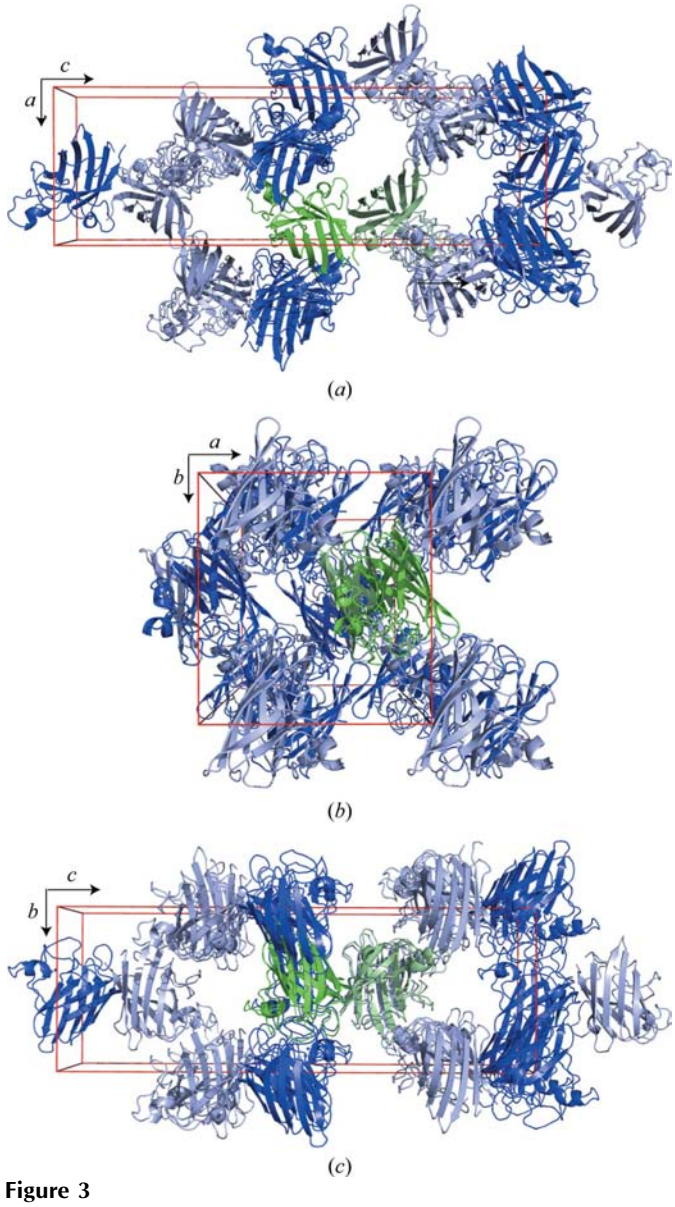

Figure 3
hpSOD intermolecular contacts in (*a*) the *ac* plane, (*b*) the *ab* plane and (*c*) the *bc* plane. Unit-cell limits are indicated in red. In (*c*) the central portion of the cell shows a protein molecule with the *A* and *B* subunits in green and light green, respectively.

scattered as the uncertainties are large. Nevertheless, the values for hpSOD are quite homogeneous and their average (2.78 Å) is slightly shorter than the average (2.82 Å) for the three structures at atmospheric pressure.

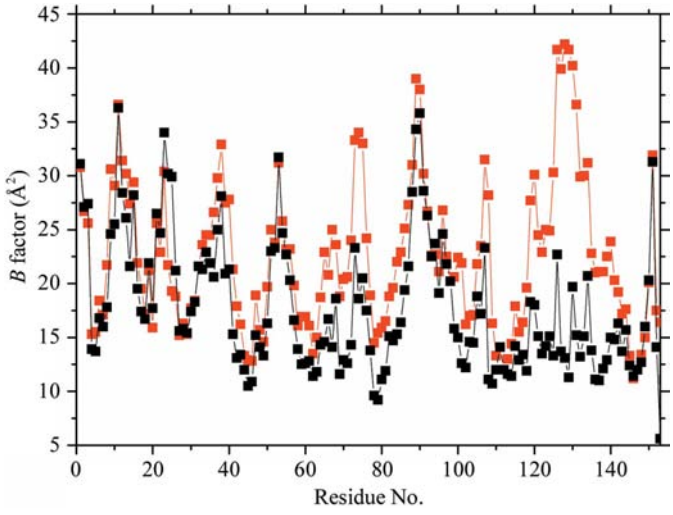

Figure 4
Equivalent isotropic *B*-factor plot as a function of residue number for subunits *A* (red) and *B* (black) of hpSOD.

3.5. Effects of pressure on subunits and intramolecular contacts

Each subunit of hpSOD is compressed with respect to the subunits of the CuCoSOD, rtSOD and ltSOD models. For hpSOD the volumes and areas of the *A* and *B* subunits are not significantly different: their values are 17 310 Å^3 and 5872 Å^2, and 17 314 Å^3 and 5875 Å^2, respectively. In contrast, all reference structures show an asymmetry between the two monomers (Table 2).

The secondary-structure elements of the *A* and *B* subunits of hpSOD are superposed in Fig. 2(*c*). The plot of positional differences *versus* residue number for hpSOD is similar to that found for rtSOD (Hough & Hasnain, 1999) and differs from those shown in Figs. 2(*a*) and 2(*b*). This indicates that both subunits are distorted by pressure in a similar way.

Peaks in the curves in Fig. 2(*c*) can be correlated with crystal contacts occurring between symmetry-equivalent molecules. In hpSOD most intermolecular contacts are between *A* and *A* subunits or *B* and *B* subunits. Turn 23–26 is in contact with loop 1 of the symmetric *A* subunit. In particular, there are two intermolecular hydrogen bonds between Asp25 and Asn63 and Ser66 of the symmetric *A* subunit. Residues 100–103 in subunit *B* are in intermolecular contact with loop 3 (residues 128–131). The majority of intermolecular contacts (Fig. 3) occur along the *a* and *b* axes rather than along the *c* axis. Most of these contacts have previously been observed at room temperature (rtSOD) and at 277 K (CuCoSOD).

In Table 4, the intermolecular distances in hpSOD and CuCoSO are compared as both structures were determined at 2 Å resolution; in the high-pressure structure all distances are systematically shorter. This anisotropic compression of the intermolecular contacts contributes to the anisotropic compression of the unit cell.

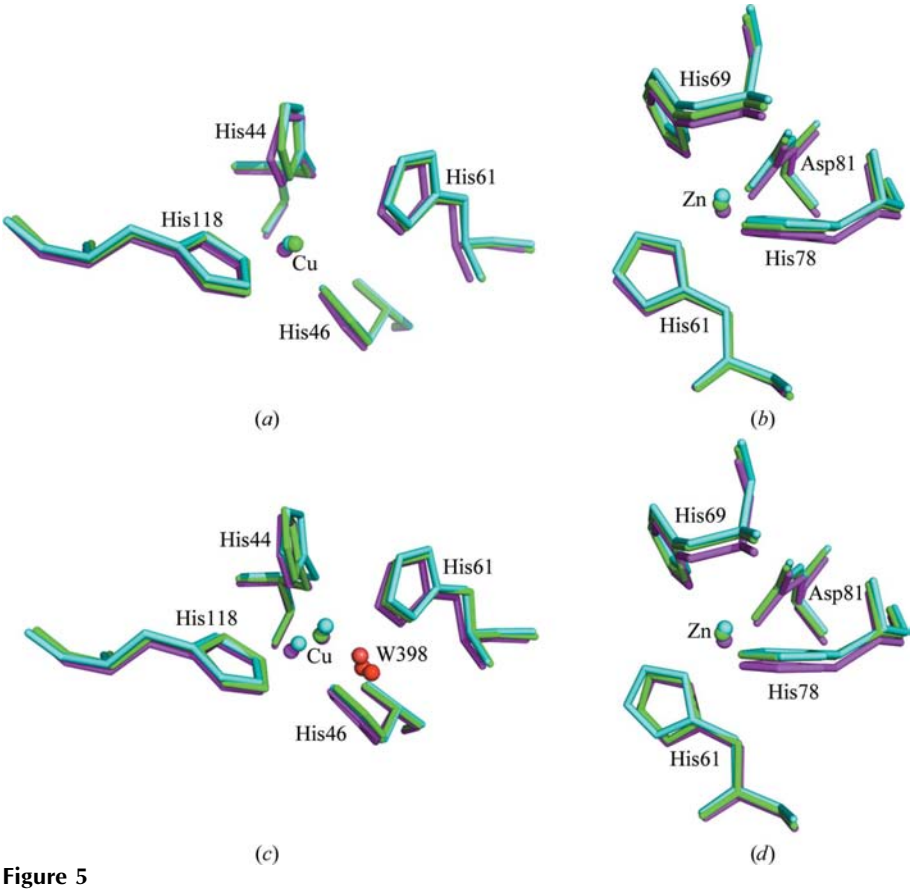

Figure 5
Superposition of hpSOD (magenta), ltSOD (cyan) and rtSOD (green) structures considering secondary-structure elements (*SSM* procedure). (*a*) *A* subunit, enlargement of the Cu site. (*b*) *A* subunit, enlargement of the Zn site. (*c*) *B* subunit, enlargement of the Cu site. (*d*) *B* subunit, enlargement of the Zn site. Water molecules are only indicated in (*c*).

3.6. Analysis of *B* factors

Fig. 4 shows the averaged temperature factor per residue as a function of residue number for the *A* and *B* subunits of hpSOD. The overall *B* value for hpSOD is 21.2 Å^2, including 206 water molecules with an average *B* value of 30.1 Å^2. The average *B* value for main chains is 19.4 Å^2. The average *B* value for side chains and 206 water molecules is 23.1 Å^2. The average *B* values for the *A* and *B* chains are 22.8 and 18.0 Å^2, respectively. Similar behaviour has been observed for rtSOD. Given that the main intermolecular

contacts are unchanged in hpSOD, a similar behaviour of the *B* factors is observed for both subunits.

3.7. Description of hpSOD metal sites

Each subunit of hpSOD contains a Cu and a Zn atom. A comparison of the metal–ligand distances in the active sites of hpSOD, rtSOD and ltSOD is given in Table 5. For both subunits in these three structures the Zn ligands are identical and are at distances that are not significantly different.

In hpSOD the Cu sites in the two subunits are not identical. The copper in the *A* subunit (Cu1) has three histidine ligands. In the *B* subunit the electron density is interpreted in terms of alternate copper positions (ACu1, occupancy 0.6; BCu, occupancy 0.4). The ACu1—BCu distance is 1.4 Å. ACu1 has three His ligands at distances shorter than 2.1 Å and His61 is at 3.2 Å. The BCu site of the *B* subunit was modelled with four histidine ligands at distances shorter than 2.3 Å plus a water ligand at 2.6 Å. An alternate Cu position in the *B* subunit has also been observed in the fully reduced structure (ltSOD). In hpSOD the water molecule in proximity to Cu in the *A* and *B* subunits has *B* factors of 21.8 and 20.2 Å^2, respectively. Several publications (Ascone *et al.*, 1997; Murphy *et al.*, 1997; Hough *et al.*, 2000) have previously analyzed the structural differences between oxidized and reduced copper sites. The copper–ligand distances for hpSOD (Cu1 in subunit *A* and ACu1 in subunit *B*) are similar to those of ltSOD (Table 5), indicating a similar Cu^{I} environment.

Fig. 5 shows details of the hpSOD, rtSOD and ltSOD metal sites after superposition of secondary-structure elements (*SSM* procedure; Emsley & Cowtan, 2004). While the coordinates of the side chains in the reduced (ltSOD) and partially reduced (rtSOD) proteins are quite similar, this is not the case for hpSOD. Fig. 5 clearly shows that with respect to reference structures hpSOD features a global shift of Cu and Zn atoms together with their ligands. Moreover, His44 and His61 in hpSOD are particularly tilted with respect to their homologues.

Table 4
Crystal contacts (Å) between symmetry-equivalent molecules in hpSOD and CuCoSOD.

		hpSOD	CuCoSOD
Asp25*A* N	Ser66*A* O	2.86	3.39
Asp25*A* OD1	Ser66*A* O	2.90	2.93
Asp25*A* OD2	Asn63*A* ND2	2.96	3.13
Glu107*A* N	Glu130*A* OE1	2.81	3.12
Asp25*B* O	Glu130*B* N	3.00	3.27
Asp25*B* OD2	Lys68*B* NZ	2.90	3.17
Leu65*B* O	Lys120*B* NZ	2.62	3.45
Pro100*B* O	Glu131*B* N	2.89	2.97
Leu101*B* O	Asn129*B* ND2	2.93	3.18
Ser103*B* OG	Gly128*B* O	2.73	2.96

Table 5
Metal–ligand distances (Å) in hpSOD, rtSOD and ltSOD.

Crystal	hpSOD			rtSOD		1q0e		
Subunit	*A*	*B*	*B*	*A*	*B*	*A*	*B*	*B*
Copper symbol	Cu1 152	ACu1 152	BCu 153				CuB152	CuA152
Cu occupancy (%)	100	60	40	100	100	100	90	10
Cu—Zn	6.78	6.86	5.88	6.59	6.08	6.87	6.87	5.97
Cu—His44	2.02	2.12	2.01	2.07	2.00	2.02	2.05	2.06
Cu—His46	2.05	1.90	2.23	2.00	2.17	1.96	2.01	2.66
Cu—His61	3.42	3.20	2.01	3.19	2.22	3.39	3.32	2.15
Cu—His118	2.03	1.91	2.31	2.03	2.19	2.08	2.04	2.42
Cu—water	3.9†	3.6†	2.6	3.50†	2.56	4.01†	3.69†	2.56
Zn—His61	2.05	1.97	—	1.97	2.02	2.05	2.05	—
Zn—His69	2.03	2.00	—	2.03	2.07	2.05	2.10	—
Zn—His78	1.96	2.09	—	2.07	1.75	2.06	2.06	—
Zn—Asp81	1.98	2.00	—	1.62	1.84	1.99	2.00	—

† These atoms are not considered to be coordinated.

4. Discussion

4.1. CuZnSOD crystal compression

CuZnSOD crystals can withstand a pressure of at least 1 GPa. This stability, which is highlighted by the detailed structural analysis at 0.57 GPa, can be related in particular to the compact secondary structure, the tight association of monomers through the broad interface, the lack of internal cavities and the presence of a disulfide bridge in each monomer (between Cys55 and Cys144). An HPMX study of hen egg-white lysozyme revealed an anisotropic compression of the tetragonal unit cell (Fourme *et al.*, 2001); an anomaly in the variation of the length of the unique axis *c* beyond 0.8 GPa coincided with a loss of diffracting power. The compression of the CuZnSOD crystal is also anisotropic. The compression along the *a* axis undergoes a significant departure from linearity at about 0.8 GPa. As the crystals are stable to a much higher pressure than 0.8 GPa, this feature is probably related to changes in structure or packing. At atmospheric pressure and low temperature (100 K) the reported unit-cell volume variation is −0.7%; the relative variations for the *a*, *b* and *c* axes are −1.7%, +0.7% and +0.3%, respectively (Hough & Hasnain, 2003). Superposition of the secondary-structure elements of the *A* and *B* subunits indicates an asymmetry between monomers at atmospheric pressure as well as at high pressure (Fig. 2*c*). Pressure modifies each subunit, but the asymmetry arising from different intermolecular *A*–*A* and *B*–*B* contacts (Fig. 3) is maintained. The two subunits in rtSOD and in hpSOD have a nearly identical distribution of temperature factors, except for residues 125–132 in the *A* subunit, which have higher *B* factors (30–42 Å^2) compared with their equivalents in the *B* subunit. This asymmetry in the *B* factors of the two monomers of CuZnSOD has been observed previously and may be related to the lack of mobility of the Glu119–Leu142 loop region in the *B* subunit caused by crystal contacts (Hough &

Hasnain, 2003; Hough *et al.*, 2000). Compared with rtSOD the volume of the whole dimer and of each subunit decreases; this volume reduction is anisotropic as the pressure affects the main chain and side chains of the molecule differently (Figs. 2*a* and 2*b*).

In conclusion, analysis of the hpSOD data indicates that the compressibility of CuZnSOD crystals is small and anisotropic. The results suggest that the anisotropic crystal compression has components that are related to packing (*i.e.* anisotropic compression of intermolecular contacts) and to protein flexibility.

4.2. Pressure and quaternary structure: crystalline CuZnSOD dimer stability

The dissociation of oligomeric proteins by pressure has been the subject of many investigations (Weber, 1993). It generally occurs at low pressures; for example, the tetrameric enzyme urate oxidase shows a typical example of such behaviour. The onset of dissociation of the quaternary structure was captured by HPMX at 0.14 GPa (Colloc'h *et al.*, 2006).

The stability of the dimer in human CuZnSOD has a medical implication: point mutations lead to the development of familial amyotrophic lateral sclerosis. Mutations located close to the dimer interface (*e.g.* Ala4Val and Ile113Thr mutants) can lead to major destabilization of human superoxide dismutase, with a substantial reorientation of the two monomers (Hough *et al.*, 2004).

Bovine CuZnSOD crystals can withstand a pressure of at least 1 GPa without significant changes in diffracting power, resolution or mosaicity, which implies that the quaternary and tertiary structures are preserved. Fluorescence measurements on solutions show that the CuZnSOD dimer from another species, *Photobacterium leiognathi*, is not dissociated at 0.65 GPa (Cioni *et al.*, 2003). These experimental results are in agreement with the large theoretical Gibbs free-energy value, -102.5 kJ mol^{-1}, for the dimer–monomer dissociation of the *P. leiognathi* superoxide dismutase (Maragliano *et al.*, 2005).

The electron density of hpSOD does not reveal signs of dimer dissociation or protein denaturation. The subunit-to-subunit backbone hydrogen bonds are identical within experimental error in the atmospheric pressure structures (rtSOD, ltSOD and CuCoSOD) and in hpSOD (Table 3).

Hummer and coworkers have proposed that pressure-dependent transfer of water entering into cavities and into hydrophobic pockets induces protein denaturation (Hummer *et al.*, 1998). The hydration of a highly hydrophobic cavity in mutated T4 lysozyme induced by pressure has been suggested to support this mechanism (Collins *et al.*, 2005). This mechanism cannot be invoked in this case as there is no indication of dimer dissociation. In hpSOD the *A* and *B* subunits display a large van der Waals contact region that avoids the formation of any cavity between the subunits. Moreover, the volume of pockets near the interface region is decreased by about 20–30%, whereas the total volume of all other pockets far from this domain is decreased by only 8%.

4.3. Pressure and tertiary structure flexibility: biological meaning of observed changes

High-pressure spectroscopic (Davydov *et al.*, 2003) and NMR (Li & Akasaka, 2006) approaches have previously been used to identify the conformational variability of proteins.

It has also been shown that thermally induced acoustic vibrations allow the estimation of mean-square atomic displacements in protein crystals (Edwards *et al.*, 1990). Data on hpSOD indicate that mean-square atomic displacements can also be produced by increasing pressure on the protein crystal.

In each hpSOD subunit, flexible regions, including large portions of the molecule such as the active-site region, have been identified at high pressure. The hpSOD structure was compared with five bovine CuZnSOD structures belonging to the same space group ($P2_12_12_1$) available in the PDB. These atmospheric pressure models are globally very similar, although they were determined at different resolutions (1.80–1.15 Å) and temperatures (100–300 K). Their main difference is the conformational variability of the Cu sites, which is associated with different oxidation states. The positional differences between superposed C$^{\alpha}$ atoms of hpSOD and of each model as a function of pressure provided ten curves with essentially the same pattern (Figs. 2*a* and 2*b* and Supplementary Figs. S2, S3 and S4). This pattern is significantly different when two model structures are superimposed (Supplementary Fig. S1).

Figs. 2(*a*) and 2(*b*) and Supplementary Figs. S2, S3 and S4 also indicate that pressure has essentially the same effect on the two subunits independent of the different intermolecular interactions formed by each subunit. As an example, we can mention the intermolecular contact between the *B* subunits involving Pro100 (in loop 2) and Gly131 (in loop 3): loop 2 is scarcely affected by pressure, in contrast to loop 3. Moreover, subunit *A* does not present this intermolecular contact but is affected by pressure similarly to the *B* subunit.

The C$^{\alpha}$-atom displacements under pressure reveal almost invariant regions such as residues at the interface region or in its proximity, as well as large flexible regions in the tertiary structure, in particular loop 3 (the so-called electrostatic loop) at the rim of the active-site cavity.

CuZnSODs from many organisms, including those living in extreme conditions such as deep seas (Teh *et al.*, 2008), have a highly conserved tertiary structure around the dimetallic sites. Their flexibility, as revealed by high-pressure measurements, may explain why CuZnSODs are found in organisms living in different conditions.

The copper-uptake process is particularly important given the role of CuZnSODs in antioxidant defence and compelling evidence that free-radical damage is involved in the pathophysiology of motor neurone disease (MND; Williams *et al.*, 2001). *In vitro* reconstitution experiments performed by X-ray absorption spectroscopy have shown that Cu$^{\mathrm{I}}$-GSH (reduced copper glutathione complex) donates copper to copper-free superoxide dismutase protein without the formation of a ternary complex in which the metal is bound to both GSH and

protein. Copper is transferred from Cu^{I}-GSH directly to the Cu-site cavity (Ascone *et al.*, 1993). This evidence led to the proposal of an uptake mechanism in which the Cu^{I}-GSH complex is attracted toward the active site of the protein, forming hydrogen bonds and salt bridges, most likely through the negative carboxyl group of GSH and the positive side chains surrounding the active site of the enzyme (Ascone *et al.*, 1993). The role of the electrostatic loop in the copper-uptake process was also supported by reconstitution experiments combined with site-directed mutagenesis, indicating that metal uptake by the mutants was much slower than by the wild-type enzyme (Ciriolo *et al.*, 2001). The soluble factor identified as *Saccharomyces cerevisiae* LYS7 and the human CCS (copper chaperone for SOD) also mediate the delivery of copper to CuZnSODs (Culotta *et al.*, 1997; Wong *et al.*, 2000). Consequently, the flexibility of the electrostatic loop as evidenced by high-pressure measurements could facilitate Cu-carrier/protein interactions and consequently copper uptake.

The investigation of metal sites using pressure allows the characterization of the conformational states involved in catalytic function. The reaction mechanism includes the cyclic reduction and oxidation of Cu by successive molecules of superoxide (Tainer *et al.*, 1983). X-ray absorption spectroscopic data recorded at the Cu *K* edge for oxidized and reduced bovine CuZnSOD in the crystalline state and in solution indicated that the active Cu ion is four-coordinated and three-coordinated by histidines in the Cu^{II} and in the Cu^{I} enzyme, respectively (Ascone *et al.*, 1997). X-ray diffraction data confirmed copper conformational variability in crystals, which is limited to the tilt of His61 and to the positions of the copper ion and of a water molecule in its proximity. In contrast, at atmospheric pressure the whole protein backbone structure and the Zn ligands were demonstrated to be essentially the same in the oxidized and reduced Cu states (Hough & Hasnain, 1999, 2003; Hough *et al.*, 2000).

In hpSOD, the C^{α} atoms of the backbone forming the cavity around the zinc are globally shifted when compared with the various models while maintaining the same Zn coordination.

As for Zn, the C^{α} atoms of the backbone around Cu are shifted with respect to the models. The two Cu sites in hpSOD are dissimilar. In the *A* subunit Cu is three-coordinated by histidines as in ltSOD. In the *B* subunit the electron density is elongated, revealing an alternate Cu position. One copper has the typical Cu^{II} coordination, while the second copper has a typical Cu^{I} coordination characterized by a lengthening of the Cu—His61 distance and an increase in the Cu–Zn separation.

The protein used in the high-pressure experiments was oxidized; consequently, the two copper sites were expected to be coordinated by four histidines.

High-pressure X-ray absorption data recorded at the Cu and Zn *K* edges on lyophilized and oxidized enzyme indicated that between 0.3 and 0.8 GPa the local structure around zinc is essentially preserved with minor modifications while a structural transition occurs at the Cu site related to a different protein conformational state (Ascone *et al.*, 2000). In X-ray absorption experiments the transition was observed at the same pressure value for several experiments independently of the exposure time to the X-ray beam, excluding any photoreduction from the experimental conditions used (I. Ascone, unpublished data). In HPMX experiments, diffraction data were recorded on several crystals, moving the crystal in front of the beam in order to irradiate successive fresh portions of the sample. The electron density and the S—S bond in each subunit support the absence of significant crystal damage. Nevertheless, *in situ* measurements combining X-ray diffraction and X-ray absorption with the same setup (Ascone *et al.*, 2006) would be required in order to define the Cu redox state with certainty. X-ray absorption experiments and the global shift of C^{α} atoms around metals involving both the main and side chains support the hypothesis that the change in Cu coordination observed in hpSOD is an effect of pressure. These results show that pressure induces a conformational variation of the active-site region.

5. Concluding remarks

The quality of the results, as evaluated by the usual indicators (*e.g.* resolution, $R_{\rm merge}$, completeness, $R_{\rm cryst}$ and $R_{\rm free}$ values), meets the usual standards of conventional macromolecular crystallography (Girard *et al.*, 2007; Fourme *et al.*, 2009) in spite of the data collection at room temperature. The present study shows that pressure is a powerful probe to investigate protein flexibility. Larger displacements are observed in more flexible zones and in such zones pressure may induce higher energy conformations that are involved in protein function.

The analysis of crystal contacts and protein structure suggests that the anisotropy in crystal compression arises from both crystal packing and protein flexibility.

The unusual stability of the dimer was investigated: at 0.57 GPa there is no sign of dissociation and the tertiary and quaternary structures are globally preserved up to at least 1 GPa. Accordingly, multimeric proteins may withstand very high pressures when the quaternary-structure interactions are particularly stable as in the case of CuZnSOD.

In hpSOD the metal-site cavities are globally shifted with respect to model structures for both subunits. Analysis of the atomic coordinates of the Glu119–Leu142 loop region involved in copper uptake confirms the flexibility of the *A* subunit and shows a similar flexibility for the *B* subunit.

The authors acknowledge the contributions of Eric Girard and Anne-Claire Dhaussy in the high-pressure measurements. The authors also acknowledge the ESRF for the provision of synchrotron-radiation facilities and the technical staff of the ID30 and ID27 beamlines for assistance during experiments, in particular Mohamed Mezouar.

References

Ascone, I., Castaner, R., Tarricone, C., Bolognesi, M., Stroppolo, M. E. & Desideri, A. (1997). *Biochem. Biophys. Res. Commun.* **241**, 119–121.

Ascone, I., Cognigni, A., Le Godec, Y. & Itie, J. P. (2000). *High Press. Res.* **19**, 667–673.

Ascone, I., Girard, E., Gourhant, P., Legrand, P., Roudenko, O., Roussier, L. & Thompson, A. W. (2006). *13th International Conference on X-ray Absorption Fine Structure – XAFS13*, pp. 872–874. New York: American Institute of Physics.
Ascone, I., Kahn, R., Girard, E., Prangé, T., Dhaussy, A.-C., Mezouar, M., Ponikwicki, N. & Fourme, R. (2010). *J. Appl. Cryst.* **43**, 407–416.
Ascone, I., Longo, A., Dexpert, H., Ciriolo, M. R., Rotilio, G. & Desideri, A. (1993). *FEBS Lett.* **322**, 165–167.
Ascone, I., Zamponi, S., Cognigni, A., Marmocchi, F. & Marassi, R. (2005). *Electrochim. Acta*, **50**, 2437–2443.
Cioni, P., Pesce, A., della Rocca, B. M., Castelli, S., Falconi, M., Parrilli, L., Bolognesi, M., Strambini, G. & Desideri, A. (2003). *J. Mol. Biol.* **326**, 1351–1360.
Ciriolo, M. R., Battistoni, A., Falconi, M., Filomeni, G. & Rotilio, G. (2001). *Eur. J. Biochem.* **268**, 737–742.
Collaborative Computational Project, Number 4 (1994). *Acta Cryst.* D**50**, 760–763.
Collins, M. D., Hummer, G., Quillin, M. L., Matthews, B. W. & Gruner, S. M. (2005). *Proc. Natl Acad. Sci. USA*, **102**, 16668–16671.
Colloc'h, N., Girard, E., Dhaussy, A. C., Kahn, R., Ascone, I., Mezouar, M. & Fourme, R. (2006). *Biochim. Biophys. Acta*, **1764**, 391–397.
Culotta, V. C., Klomp, L. W. J., Strain, J., Casareno, R. L. B., Krems, B. & Gitlin, J. D. (1997). *J. Biol. Chem.* **272**, 23469–23472.
Davydov, D. R., Halpert, J. R., Renaud, J. P. & Hoa, G. H. B. (2003). *Biochem. Biophys. Res. Commun.* **312**, 121–130.
Djinovic, K., Coda, A., Antolini, L., Pelosi, G., Desideri, A., Falconi, M., Rotilio, G. & Bolognesi, M. (1992). *J. Mol. Biol.* **226**, 227–238.
Dundas, J., Ouyang, Z., Tseng, J., Binkowski, A., Turpaz, Y. & Liang, J. (2006). *Nucleic Acids Res.* **34**, W116–W118.
Edwards, C., Palmer, S. B., Emsley, P., Helliwell, J. R., Glover, I. D., Harris, G. W. & Moss, D. S. (1990). *Acta Cryst.* A**46**, 315–320.
Emsley, P. & Cowtan, K. (2004). *Acta Cryst.* D**60**, 2126–2132.
Fourme, R., Girard, E., Kahn, R., Dhaussy, A.-C. & Ascone, I. (2009). *Annu. Rev. Biophys.* **38**, 153–171.
Fourme, R., Girard, E., Kahn, R., Dhaussy, A.-C., Mezouar, M., Colloc'h, N. & Ascone, I. (2006). *Biochim. Biophys. Acta*, **1764**, 384–390.
Fourme, R., Kahn, R., Mezouar, M., Girard, E., Hoerentrup, C., Prangé, T. & Ascone, I. (2001). *J. Synchrotron Rad.* **8**, 1149–1156.
Fridovich, I. (1975). *Annu. Rev. Biochem.* **44**, 147–159.
Girard, E., Dhaussy, A.-C., Couzinet, B., Chervin, J.-C., Mezouar, M., Kahn, R., Ascone, I. & Fourme, R. (2007). *J. Appl. Cryst.* **40**, 912–918.
Guex, N. & Peitsch, M. C. (1997). *Electrophoresis*, **18**, 2714–2723.
Hough, M. A., Grossmann, J. G., Antonyuk, S. V., Strange, R. W., Doucette, P. A., Rodriguez, J. A., Whitson, L. J., Hart, P. J., Hayward, L. J., Valentine, J. S. & Hasnain, S. S. (2004). *Proc. Natl Acad. Sci. USA*, **101**, 5976–5981.
Hough, M. A. & Hasnain, S. S. (1999). *J. Mol. Biol.* **287**, 579–592.
Hough, M. A. & Hasnain, S. S. (2003). *Structure*, **11**, 937–946.
Hough, M. A., Strange, R. W. & Hasnain, S. S. (2000). *J. Mol. Biol.* **304**, 231–241.
Hummer, G., Garde, S., Garcia, A. E., Paulaitis, M. E. & Pratt, L. R. (1998). *Proc. Natl Acad. Sci. USA*, **95**, 1552–1555.
Kabsch, W. (1993). *J. Appl. Cryst.* **26**, 795–800.
Kabsch, W. & Sander, C. (1983). *Biopolymers*, **22**, 2577–2637.
Laskowski, R. A., MacArthur, M. W., Moss, D. S. & Thornton, J. M. (1993). *J. Appl. Cryst.* **26**, 283–291.
Li, H. & Akasaka, K. (2006). *Biochim. Biophys. Acta*, **1764**, 331–345.
Maragliano, L., Falconi, M., Sergi, A., Cioni, P., Castelli, S., Lania, A., Stroppolo, M. E., Strambini, G., Ferrario, M. & Desideri, A. (2005). *Biophys. J.* **88**, 2875–2882.
Murphy, L. M., Strange, R. W. & Hasnain, S. S. (1997). *Structure*, **5**, 371–379.
Murshudov, G. N., Vagin, A. A. & Dodson, E. J. (1997). *Acta Cryst.* D**53**, 240–255.
Nordlund, A. & Oliveberg, M. (2006). *Proc. Natl Acad. Sci. USA*, **103**, 10218–10223.
Schneider, T. R. (2002). *Acta Cryst.* D**58**, 195–208.
Tainer, J. A., Getzoff, E. D., Beem, K. M., Richardson, J. S. & Richardson, D. C. (1982). *J. Mol. Biol.* **160**, 181–217.
Tainer, J. A., Getzoff, E. D., Richardson, J. S. & Richardson, D. C. (1983). *Nature (London)*, **306**, 284–287.
Teh, A.-H., Kanamasa, S., Kajiwara, S. & Kumasaka, T. (2008). *Biochem. Biophys. Res. Commun.* **374**, 475–478.
Vallone, B., Nienhaus, K., Matthes, A., Brunori, M. & Nienhaus, G. U. (2004). *Proc. Natl Acad. Sci. USA*, **101**, 17351–17356.
Weber, G. (1993). *J. Phys. Chem.* **97**, 7108–7115.
Williams, R. E., Cookson, M. R., Fray, A. E., Manning, P. M., Menzies, F. M., Figlewicz, D. A. & Shaw, P. J. (2001). *Neurosci. Lett.* **302**, 146–150.
Wong, P. C., Waggoner, D., Subramaniam, J. R., Tessarollo, L., Bartnikas, T. B., Culotta, V. C., Price, D. L., Rothstein, J. & Gitlin, J. D. (2000). *Proc. Natl Acad. Sci. USA*, **97**, 2886–2891.